Lagrangian Dynamics in Plane Couette Turbulence

John R. Elton[*1], Predrag Cvitanović[†1], John F. Gibson[1], and Jonathan Halcrow[1]

[1]Center for Nonlinear Science, School of Physics, Georgia Institute of Technology, Atlanta, GA

Abstract

The behavior of tracer particle trajectories for invariant solutions of the Navier-Stokes equations confined to the three-dimensional geometry of plane Couette flow is studied. Treating an equilibrium velocity field as a dynamical system, the transport of these passive scalars along flow trajectories within the field reveals coherent structures in the Lagrangian frame that form a basic outline for the different types of motion that can occur. Using analytic arguments that make use of the symmetry of the plane Couette geometry, we uncover special points in the velocity field for which where there is no fluid movement. We numerically determine the stability of these points of stagnation along with their stable and unstable manifolds, and also find heteroclinic connections between them. These topological features provide a structured phase portrait that outlines the $3D$ Lagrangian flow dynamics for a turbulent fluid, which may be used as a first step to studying a wide range of bulk fluid properties related to particle transport and advective mixing.

Keywords– turbulence, mixing, plane Couette flow, Navier-Stokes

1   Introduction

The turbulent transport and mixing of different particles or species within a fluid is a problem with both wide practical application as well as theoretical interest, yet a complete understanding of the phenomena remains elusive; even questions related to how we define or measure various mixing properties are not universally agreed upon. In [1], some pitfalls of standard approaches such as measuring variation from homogeneity with an L^2 or L^p norm, or computing the entropy of the underlying dynamical system, are pointed out. Furthermore, there are experimental and computational challenges involved when studying the problem in the natural Lagrangian frame [2, 3, 4, 5]. Although the idea of taking a dynamical systems approach to the problem is not new, as books by Ottino [6] and Wiggins [7] attest to the value of using invariant manifolds to study fluid transport, [2] and [8] point out that Lagrangian coherent structures in real flow data are difficult to identify due to the uncertain stability of individual particles. Thus many of the theoretical and experimental analyses are confined to *two-dimensional* systems, with a large body of the work on Lagrangian dynamics focusing on the statistical properties and fluctuations of particle velocities, and on detecting intermittency or anomalous scaling laws [9, 5, 3, 10].

In this study, we extend the idea of looking at the Lagrangian transport of passive scalars by means of the invariant structures within the flow in a *truly $3D$ system*, partitioning the physical space of the fluid in a way that reveals distinct types of motion that can occur, driving the organization of tracer mixing [8]. By building upon the computational work that has provided exact invariant solutions of the fully resolved Navier-Stokes equations for plane Couette flow, described below, we are able to use equilibrium velocity field solutions to study a tractable, yet still complex problem that lends itself to a dynamical systems analysis. Symmetry considerations allow for a first tangible step that will lead to piecing together a full phase portrait of such an equilibrium flow, by determining the fixed points and their stabilities along with heteroclinic connections. Our eventual goal is then putting this information together to assist in understanding how to calculate quantities to best characterize turbulent fluid mixing.

The plane Couette geometry we study is a shear flow in which two infinite plates move in opposite directions at constant speed, with turbulent behavior beginning to set in approximately above Reynolds number $Re = 325$ [11]. Eulerian equilibrium velocity fields have been computed for this setup over a number of years, and plane Couette flow also admits periodic, relative periodic, and traveling wave solutions

---

[*]Jelton.physics@gmail.com
[†]predrag@gatech.edu

[11, 12]. In 1990 Nagata [13] discovered what are known as the Upper Branch and Lower Branch equilibria by continuing a known solution from Taylor-Couette flow to plane Couette. Later, Waleffe [14] calculated the same solutions a different way and noted that they satisfy 'shift-rotate' and 'shift-reflect' symmetry. Gibson et al. [15] began explorations of plane Couette dynamics around those equilibria, making use of the symmetries and noting that the subspace of velocity fields under the action of certain symmetry groups was invariant under Navier-Stokes. The search for new invariant solutions focused on this subspace, from which a Newton search was able to detect more equilibria. The reader may consult [11] or [15] for additional history of the computational discoveries of invariant solutions for plane Couette flow.

Much of the analysis in this work is carried out on a particular equilibrium solution referred to as the Upper Branch or EQ_2. We also repeat some of our analysis for another equilibrium velocity field EQ_8, for which the flow is more turbulent and possesses different invariant symmetries. For analyzing fluid particle trajectories from the Lagrangian perspective, where we follow the motion of a tracer within a fixed equilibrium, we need to make a distinction between $3D$ physical fluid flow for a given invariant solution of Navier-Stokes and the dynamical ∞-dimensional state space flow. We distinguish between the two by using physically motivated nomenclature for the $3D$ physical fluid flow: We shall refer to the position for which $\mathbf{u}(\mathbf{x}_{SP}) = 0$ as the *stagnation point* $\mathbf{x}_{SP}$ or point SP. And when we discuss coherent structures and heteroclinic connections, these again refer to trajectories *within* a known Eulerian equilibrium velocity field, in contrast to the heteroclinic connections described in, for example [11], which track the evolution of the velocity fields themselves.

In sect. 2.1-sect. 2.3 we review the underlying equations and geometry for plane Couette flow, describe how the equilibria are stored numerically for use in computing Lagrangian trajectories, and give a deep dive on the symmetries which are crucial for later analysis. Much of the information in these sections is a rehash that can be found in other places including [15], but is important for understanding the new contributions of this work. In sect. 2.4 we show how the known symmetries automatically provide us with critical information for analyzing Lagrangian trajectories within each equilibrium by determining where the velocity field must be exactly 0; in other words we are able to locate the "fixed points" in dynamical systems terminology, or stagnation points in our lingo. In sect. 3 we give our core analysis and results: namely a dynamical systems treatment of Lagrangian trajectories within plane Couette equilibria that includes a treatment of fixed points, stability analysis and invariant manifolds, and heteroclinic connections, providing the basic dynamical skeleton through which transport and mixing properties in a turbulent flow field may be analyzed. We provide an intriguing graphical phase portrait of the turbulent motion within the Upper Branch equilibrium and also provide some results for EQ_8 and discuss potential applications.

2 Plane Couette Flow

2.1 The Navier-Stokes equations

The underlying equations that govern the motion of plane Couette flow are the Navier-Stokes equations, along with boundary conditions. The boundary conditions for plane Couette flow in the x and z directions are periodic, $\mathbf{u}(x, y, z) = \mathbf{u}(x + L_x, y, z) = \mathbf{u}(x, y, z + L_z)$. In the y direction, $\mathbf{u} = (1, 0, 0)$ at $\mathbf{x} = (0, 1, 0)$ and $\mathbf{u} = (-1, 0, 0)$ at $\mathbf{x} = (0, -1, 0)$.

The fluid is taken to be incompressible, so in this case the Navier-Stokes equations are

$$\frac{\partial \mathbf{u}}{\partial t} + (\mathbf{u} \cdot \nabla)\mathbf{u} = -\nabla p + \frac{1}{Re}\nabla^2 \mathbf{u}, \qquad \nabla \cdot \mathbf{u} = 0. \tag{1}$$

For an equilibrium velocity field that is not changing in time, the first equation in (1) simplifies to

$$(\mathbf{u} \cdot \nabla)\mathbf{u} = -\nabla p + \frac{1}{Re}\nabla^2 \mathbf{u}, \tag{2}$$

The Reynolds number parameter *Re*, which gives a measure of fluid viscosity and degree to which fluid motion may become turbulent, is given by

$$Re = \frac{\overline{u}L}{\nu} \tag{3}$$

where $\overline{u}$ is the average fluid velocity and L is the characteristic length. Thus the form of the Navier-Stokes equations and boundary conditions make use of rescaling to use non-dimensionalized variables. We use $Re = 400$, in the regime of moderate turbulence, for the plane Couette flow simulations throughout the text unless otherwise indicated.

In most of our work, velocity field $\mathbf{u}$ represents the *difference* from the laminar flow. So we can break up the total velocity field into two components: $\mathbf{u_{tot}} = y\hat{\mathbf{x}} + \mathbf{u}$. Here $y\hat{\mathbf{x}}$ is the laminar velocity field and $\mathbf{u}$ is then the difference between the total velocity and laminar. Substitute $y\hat{\mathbf{x}} + \mathbf{u}$ for $\mathbf{u}$ in the nondimensionalized Navier-Stokes equations above to get

$$\frac{\partial \mathbf{u}}{\partial t} + y\frac{\partial \mathbf{u}}{\partial x} + v\,\hat{\mathbf{x}} + \mathbf{u} \cdot \nabla \mathbf{u} = -\nabla p + \frac{1}{Re}\nabla^2 \mathbf{u}, \quad \nabla \cdot \mathbf{u} = 0 \tag{4}$$

with boundary conditions $\mathbf{u} = 0$ at $y \pm 1$. The equilibrium velocity fields we study satisfy (4). This equation is a little more complicated than (1), but having Dirichlet boundary conditions on $\mathbf{u}$ makes the analysis much easier, since the set of allowable velocity fields (those fields that satisfy incompressibility and boundary conditions) forms a vector space.
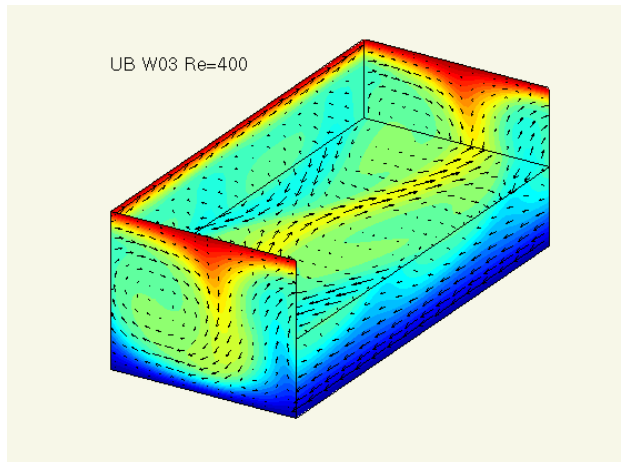

Figure 1: Visualization of the Upper Branch equilibrium velocity field, from `Channelflow.org`.

2.2 Computation of trajectories from equilibrium velocity fields

In order to integrate streamlines of plane Couette flow and follow the paths of tracer particles, it is first necessary to have numerically accurate equilibrium $3D$-velocity fields.

The starting point for this task is to obtain the necessary data sets for evaluating velocity field values for a given equilibrium, e.g. the Upper Branch as shown in figure 1. These are made available at the website `Channelflow.org` [16]. The data obtained [17] stores the spectral coefficients $\hat{\mathbf{u}}$ of the expansion of a velocity field $\mathbf{u}(\mathbf{x})$. The form of the expansion is

$$\mathbf{u}(\mathbf{x}) = \sum_{m_y=0}^{M_y-1} \sum_{m_x=0}^{M_x-1} \sum_{m_z=0}^{M_z-1} \hat{\mathbf{u}}_{m_x,m_y,m_z} \bar{T}_{m_y}(y) e^{2\pi i(k_x x/L_x + k_z z/L_z)} + \text{(c.c.)} \tag{5}$$

The $\bar{T}(y)$'s are Chebyshev polynomials defined on the interval [a,b] (in most cases [-1,1]). For a given velocity field expansion, the upper bounds on the sums are known from the geometry, and the k's are related to the m's through the following relations:

$$k_x = \begin{cases} m_x & 0 \le m_x \le M_x/2 \\ m_x - M_x & M_x < m_x < M_x \end{cases} \tag{6}$$

$$k_z = m_z \qquad 0 \le m_z < M_z. \tag{7}$$

Hence, with a knowledge of the spectral coefficients we can compute $\mathbf{u}(\mathbf{x})$ by evaluating this sum at a particular $\mathbf{x} = (x, y, z)$.

Various internal functions within `Channelflow.org` have been written to compute $\mathbf{u}$ on a set of gridpoints. It is possible, by interpolation of the velocity fields on these gridpoint values, to integrate a trajectory with great computational speed. However this will not be nearly as accurate as evaluating the sum (5) directly. So we evaluate (5) to give the exact velocity field at every point along a trajectory. We are able to perform these computations in Matlab with enough speed to compute many tracer particle trajectories within an equilibrium velocity for an adequate length of time to study the flow dynamics. The code has been checked to be correct by picking an (x, y, z) coordinate that *happens* to lie on a gridpoint value and then comparing the result to the value given by the internal `Channelflow.org` functions.

2.3 Symmetries of plane Couette flow

As part of our theoretical analysis of trajectories of fluid particles within an equilibrium velocity field, it will be critical to use and understand the symmetries involved in the special geometry of plane Couette flow. Thus we take a quick detour to discuss these symmetries from a group-theoretic perspective. We focus on the symmetries relevant to the equilibria studied in this work; additional details are provided in [18].

3

Plane Couette flow is invariant under two reflections σ_1, σ_2 and a continuous two-parameter group of translations $\tau(d_x, d_z)$:

$$
\begin{aligned}
\sigma_1\,[u, v, w](x, y, z) &= [u, v, -w](x, y, -z) \\
\sigma_2\,[u, v, w](x, y, z) &= [-u, -v, w](-x, -y, z) \\
\tau(d_x, d_z)[u, v, w](x, y, z) &= [u, v, w](x + d_x, y, z + d_z)\,.
\end{aligned}
\tag{8}
$$

The Navier-Stokes equations and boundary conditions are invariant for any symmetry s in the group generated by these elements: $\partial(s\mathbf{u})/\partial t = s(\partial \mathbf{u}/\partial t)$.

The plane Couette symmetries can be interpreted geometrically in the space of fluid velocity fields. Let $\mathbb{U}$ be the space of square-integrable, real-valued velocity fields that satisfy the kinematic conditions of plane Couette flow:

$$
\begin{aligned}
\mathbb{U} = \{\mathbf{u} \in L^2(\Omega) \mid \nabla \cdot \mathbf{u} = 0,\ \mathbf{u}(x, \pm 1, z) = 0, \\
\mathbf{u}(x, y, z) = \mathbf{u}(x + L_x, y, z) = \mathbf{u}(x, y, z + L_z)\}\,.
\end{aligned}
\tag{9}
$$

The continuous symmetry $\tau(d_x, d_z)$ maps each state $\mathbf{u} \in \mathbb{U}$ to a $2D$ torus of states with identical dynamic behavior. This torus in turn is mapped to four equivalent tori by the subgroup $\{1, \sigma_1, \sigma_2, \sigma_1\sigma_2\}$. In general a given state in $\mathbb{U}$ has four $2D$ tori of dynamically equivalent states.

Most of the Eulerian equilibria that are currently known for plane Couette flow are invariant under the 'shift-reflect' symmetry $s_1 = \tau(L_x/2, 0)\,\sigma_1$ and the 'shift-rotate' symmetry $s_2 = \tau(L_x/2, L_z/2)\,\sigma_2$. These symmetries form a group

$$
S = \{1, s_1, s_2, s_3\}, \qquad s_3 = s_1 s_2,
\tag{10}
$$

which is isomorphic to the Abelian dihedral group D_2, and is a subgroup of a larger group generated by plane Couette symmetries. The group acts on velocity fields as:

$$
\begin{aligned}
s_1\,[u, v, w](x, y, z) &= [u, v, -w](x + L_x/2,\ y,\ -z) \\
s_2\,[u, v, w](x, y, z) &= [-u, -v, w](-x + L_x/2,\ -y,\ z + L_z/2) \\
s_3\,[u, v, w](x, y, z) &= [-u, -v, -w](-x,\ -y,\ -z + L_z/2)
\end{aligned}
\tag{11}
$$

We denote the S-invariant subspace of states invariant under symmetries (11) by

$$
\mathbb{U}_c = \{\mathbf{u} \in \mathbb{U} \mid s_j \mathbf{u} = \mathbf{u},\ \ s_j \in S\}\,,
\tag{12}
$$

where $\mathbb{U}_c \subset \mathbb{U}$. $\mathbb{U}_c$ is a flow-invariant subspaces: states initiated in it remain there under the Navier-Stokes dynamics.

Translations of half the cell length in the spanwise and/or streamwise directions commute with S. These operators generate a discrete subgroup of the continuous translational symmetry group $SO(2) \times SO(2)$:

$$
T = \{e, \tau_x, \tau_z, \tau_{xz}\}, \qquad \tau_x = \tau(L_x/2, 0)\,, \ \tau_z = \tau(0, L_z/2)\,, \ \tau_{xz} = \tau_x \tau_z\,.
\tag{13}
$$

Since the action of T commutes with that of S, the three half-cell translations $\tau_x \mathbf{u}$, $\tau_z \mathbf{u}$, and $\tau_{xz} \mathbf{u}$ of $\mathbf{u} \in \mathbb{U}_c$ are also in $\mathbb{U}_c$.

We know that the equilibria EQ_1-EQ_8 are symmetric in S because they satisfy those symmetries numerically. There is no a priori reason that the equilibria should be S-symmetric, other than S symmetry fixes x, z phase and so rules out relative equilibria. But s_3 symmetry alone does the same, and a few equilibria are known that have s_3 symmetry but neither s_1 nor s_2 symmetry. There are equilibria with other symmetries that fix x, z phase but have other translations than the half-cell shifts.

It is also possible to form other isotropy subgroups from the plane Couette symmetries $\tau_x, \tau_z, \sigma_1, \sigma_2$. These elements generate a group G of order 16, of which there are various subgroups of possible orders $\{1, 2, 4, 8, 16\}$. It is known that other equilibria posses different symmetries, corresponding to different subgroups of G. For example, for equilibrium EQ_8, we find there is symmetry under an invariance group of order 8, denoted S_8, that is isomorphic to the dihedral group D_4.

$$
S_8 = \{e, s1, s2, s3, s4, s5, s6, s7\}
\tag{14}
$$

where $s_4 = \tau_z\,\sigma_1$, $s_5 = s_4 s_2$, $s_6 = \tau_x \tau_z$, $s_7 = \sigma_2$. The action of these additional symmetries of S_8 on velocity fields is:

$$
\begin{aligned}
s_4\,[u, v, w](x, y, z) &= [u, v, -w](x,\ y,\ -z + L_z/2) \\
s_5\,[u, v, w](x, y, z) &= [-u, -v, -w](-x + L_x/2,\ -y,\ -z) \\
s_6\,[u, v, w](x, y, z) &= [u, v, w](x + L_x/2,\ y,\ z + L_z/2) \\
s_7\,[u, v, w](x, y, z) &= [-u, -v, w](-x,\ -y,\ z)
\end{aligned}
\tag{15}
$$

Which symmetries happen to exist for the different equilibria will have important implications for studying the dynamics of the flow.

4

2.4 Symmetry and Stagnation Points

From the form of s_3 in (11), we can see that any Eulerian equilibrium that is invariant under S has 4 Lagrangian stagnation points at which the velocity is 0, which satisfy the condition:

$$(x, y, z) = (-x, -y, -z + L_z/2) \tag{16}$$

There are 4 points which satisfy this constraint:

$$
\begin{aligned}
\mathbf{x}_{SP_1} &= (L_x/2, 0, L_z/4) \\
\mathbf{x}_{SP_2} &= (L_x/2, 0, 3L_z/4) \\
\mathbf{x}_{SP_3} &= (0, 0, L_z/4) \\
\mathbf{x}_{SP_4} &= (0, 0, 3L_z/4) .
\end{aligned} \tag{17}
$$

We refer to these as stagnation points SP_1-SP_4. Due to the periodic boundary conditions, we equivalently have $(L_x, 0, L_z/4) = SP_3$ and $(L_x, 0, 3L_z/4) = SP_4$. Also of note is the fact that there can exist no s_3-invariant relative equilibria, since s_3 operation flips both the x and z axes. These stagnation points will exist in all of the equilibria with S-symmetry. Additionally, for an equilibrium such as EQ_8 which possesses S_8 symmetry, from the action of s_5 in (15), we will find stagnation points wherever

$$(x, y, z) = (-x + L_x/2, -y, -z) \tag{18}$$

which gives the additional points:

$$
\begin{aligned}
\mathbf{x}_{SP_5} &= (L_x/4, 0, 0) \\
\mathbf{x}_{SP_6} &= (3L_x/4, 0, 0) \\
\mathbf{x}_{SP_7} &= (L_x/4, 0, L_z/2) \\
\mathbf{x}_{SP_8} &= (3L_x/4, 0, L_z/2) .
\end{aligned} \tag{19}
$$

In fact, we can generalize the discussion. Looking at the way the plane Couette symmetries act on velocity fields in (8), we see that since τ does not affect the velocity components, the condition needed to produce a stagnation point (in which all three velocity components are negated at some shifted position) will work only for the combinations of these elements which contain both σ_1 and σ_2 an odd number of times. Within the group G of order 16 of plane Couette symmetries generated by $\sigma_1, \sigma_2, \tau_x, \tau_z$, the requirement means we just have to identify elements that have a $\sigma_1\sigma_2$ term.

There are in fact four such elements of G that contain a $\sigma_1\sigma_2$ term. We denote these as $g_1 = \sigma_1\sigma_2$, $g_2 = \sigma_1\sigma_2\tau_x$, $g_3 = \sigma_1\sigma_2\tau_z$, and $g_4 = \sigma_1\sigma_2\tau_x\tau_z$.

$$g_1 [u, v, w](x, y, z) = [-u, -v, -w](-x, -y, -z) \tag{20}$$

$$g_2 [u, v, w](x, y, z) = [-u, -v, -w](-x + L_x/2, -y, -z) \tag{21}$$

$$g_3 [u, v, w](x, y, z) = [-u, -v, -w](-x, -y, -z + L_z/2) \tag{22}$$

$$g_4 [u, v, w](x, y, z) = [-u, -v, -w](-x + L_x/2, -y, -z + L_z/2) \tag{23}$$

Different isotropy subgroups of G may or may not contain a symmetry which corresponds to one of these g_1-g_4 elements, however any g_i that is part of an invariance group for an equilibrium implies the existence of four symmetrically-located stagnation points in the $y = 0$ plane. Note that g_3 and g_2 are the elements already discussed that produce SP_1-SP_8.

Any equilibrium with g_1 symmetry implies that there would additionally be stagnation points at $(0, 0, 0)$, $(L_x/2, 0, 0)$, $(0, 0, L_z/2)$, and $(L_x/2, 0, L_z/2)$. And similarly, g_4 symmetry implies the existence of stagnation points at $(L_x/4, 0, L_z/4)$, $(L_x/4, 0, 3L_z/4)$, $(3L_x/4, 0, L_z/4)$, and $(3L_x/4, 0, 3L_z/4)$. The set of all possible stagnation points based on various plane Couette flow symmetries is shown in figure 2.

So the question of existence of stagnation points for a given equilibrium is, which of the g_i symmetries does that equilibrium possess? This is a question related to invariance under the isotropy subgroups. Of importance, this does not address the question of whether *other* nontrivial stagnation points may exist that are not based on symmetry arguments alone. For the known equilibria of plane Couette flow EQ_1-EQ_{11}, all of them have g_3 symmetry and EQ_7, EQ_8 additionally have g_2 symmetry. This is likely related to the fact that searches for equilibria were done in a symmetric subspace which contained the g_3 elements (the S-symmetric subspace).

2.5 Proof that any new stagnation point must have a partner, symmetric about one of the previously known stagnation points

Though our symmetry arguments do not determine whether or not there may exist *additional* stagnation points which are not forced by the g_i symmetries in the preceding section, we can in fact that show that for
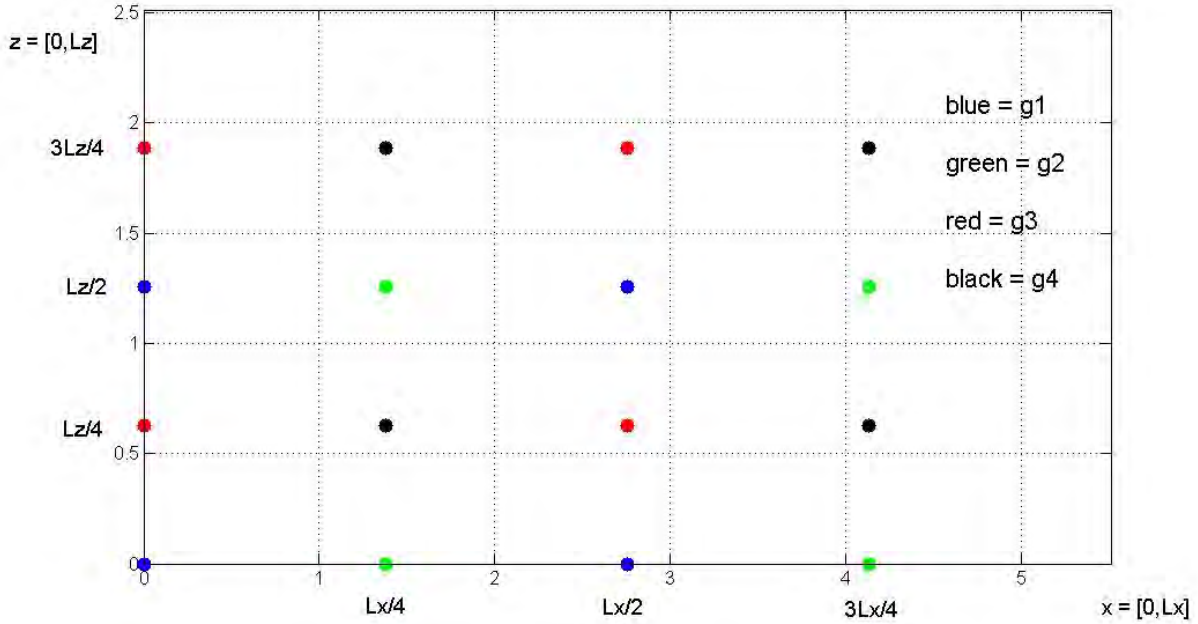
Figure 2: Sets of possible stagnation points. If one of the g_i symmetries is possessed, the velocity field will have stagnation points of the color corresponding to that symmetry.

equilibria which exist in one of the flow-invariant subspaces that contains a g_i-symmetry (for example, S has g_3 symmetry and S_8 has both g_2 and g_3 symmetry), any additional nontrivial stagnation points that exist must occur in symmetric pairs centered around the other known stagnation points.

Consider one of the equilibria in the S-invariant subspace, such as EQ_2. Again, the action of $s_3 \in S$ on velocity fields gives:

$$s_3 \left[u, v, w\right](x, y, z) = [-u, -v, -w](-x, -y, -z + L_z/2).$$

If (x_{SP}, y_{SP}, z_{SP}) is a stagnation point, $[u, v, w](x_{SP}, y_{SP}, z_{SP}) = [0, 0, 0]$, then

$$
\begin{aligned}
s_3 \left[u, v, w\right](x_{SP}, y_{SP}, z_{SP}) &= [-u, -v, -w](-x_{SP}, -y_{SP}, -z_{SP} + L_z/2) \\
&= [0, 0, 0](-x_{SP}, -y_{SP}, -z_{SP} + L_z/2). \quad (24)
\end{aligned}
$$

Thus $(-x_{SP}, -y_{SP}, -z_{SP} + L_z/2)$ is also a stagnation point.
We may parameterize a line passing through two points $(x_1, y_1, z_1), (x_2, y_2, z_2)$ as

$$x = x_1 + (x_2 - x_1)t \quad (25)$$
$$y = y_1 + (y_2 - y_1)t \quad (26)$$
$$z = z_1 + (z_2 - z_1)t \quad (27)$$
$$t \in (-\infty, \infty) \quad (28)$$

Using the two stagnation points (x_{SP}, y_{SP}, z_{SP}) and $(-x_{SP}, -y_{SP}, -z_{SP} + L_z/2)$ this becomes

$$x = x_{SP}(1 - 2t) \quad (29)$$
$$y = y_{SP}(1 - 2t) \quad (30)$$
$$z = z_{SP}(1 - 2t) + \frac{L_z}{2}t \quad (31)$$

When $t = 1/2$ this system returns $(x, y, z) = (0, 0, L_z/4)$, showing that SP_3 lies on the line between these two stagnation points, halfway in between them.

If we invoke the box periodicities: $x = x + L_x$, $z = z + L_z$, it is easy to show that this pair of stagnation points is also symmetric about any of SP_1-SP_4. For example,

x = x + L$_\mathbf{x}$:
(x_{SP}, y_{SP}, z_{SP}) is a stagnation point $\Rightarrow (-x_{SP} + L_x, -y_{SP}, z_{SP} + L_z/2)$ a stagnation point.

$$x = x_{SP}(1 - 2t) + L_x t \quad (32)$$
$$y = y_{SP}(1 - 2t) \quad (33)$$
$$z = z_{SP}(1 - 2t) + \frac{L_z}{2}t \quad (34)$$

6

When $t = 1/2$ this returns $(x, y, z) = (L_x/2, 0, L_z/4)$, so that the new stagnation points lie symmetrically on a line passing through SP_1.

For an equilibrium invariant under S_8, such as EQ_8, existence of any additional nontrivial stagnation point will then imply *two* additional stagnation points, based on the action of g_2 and g_3. If (x_{SP}, y_{SP}, z_{SP}) is a stagnation point, then $(-x_{SP}, -y_{SP}, -z_{SP} + L_z/2)$ and $(-x_{SP} + L_x/2, -y_{SP}, -z_{SP})$ are also stagnation points.

We will investigate numerical methods to determine the possible existence of any nontrivial stagnation points. In fact for EQ_2, as we show in the next section, we do find such a point and it's symmetric partner. These additional stagnation points are critical for understanding the flow dynamics in the equilibrium field, as their stable and unstable manifolds provide us with an outline of the overall dynamics.

3   Lagrangian Dynamics

We know of the existence of stagnation points in the flow of an equilibrium velocity field predicted from the symmetries of plane Couette flow. Thus the starting point for our investigation is clear; treating an equilibrium velocity field as an autonomous dynamical system we have already identified the "fixed points" of the system, which we refer to in this context as the stagnation points. Using the sum formula for computing velocities at any point in the plane Couette flow domain (5), by differentiating this formula it is a simple matter to compute the [3×3] velocity gradients or Jacobian matrix at any point. Eigenvalues and eigenvectors of this matrix will provide linear stability analysis results for the stagnation points, and allow us to compute and visualize the local stable and unstable manifolds by starting a collection of tracer points along the directions of the eigenvectors, integrating them forwards and backwards in time (when the local tangent space is $2D$, trajectories are started throughout a small radius in the plane spanned by the eigenvectors). Though this method may underrepresent a part of the manifold for the $2D$ case [19], we find that the approximation works for revealing the interesting and relevant dynamical behaviors we seek.

In order to investigate additional locations in the domain for which no movement occurs, we may numerically compute $|\mathbf{u}|^2$ along a fine grid and try to ascertain regions where the velocity value falls below a given threshold. Then, using interpolation within these regions, any additional stagnation points can be pinned down.

With the determination of the stagnation points and their invariant manifolds, we find a natural way to view the physical space of the fluid, partitioned into regions wherein the dynamics is dominated by the trajectories following closely to the manifolds themselves. This provides us with a framework for studying how transport may occur within and between the different regions.

3.1   A colorful portrait of the Upper Branch equilibrium

Our analysis is carried out for the Upper Branch equilibrium velocity field, EQ_2, at $Re = 400$. The cell size parameters are

$$[L_x, 2, L_z] = [2\pi/1.14, 2, 4\pi/5] \ [5.512, 2, 2.513]. \tag{35}$$

To begin, we look at the evolution of Lagrangian tracers starting on a grid of points, shown in figure 3. The grid is chosen to lie in the $[y, z]$ plane, centered at $x = L_x/2$. The initial points are equally spaced, and offset by one position from the edge of the box. If the number of points is chosen to be one less than a multiple of 4, there will be points starting at $\mathbf{x}_{SP_1} = (L_x/2, 0, L_z/4)$ and $\mathbf{x}_{SP_2} = (L_x/2, 0, 3L_z/4)$. The trajectories are integrated and run for a relatively short time. Here, the tracers are shown for $\mathbf{u}$ defined as the difference from laminar flow. Just from evolving the grid of points alone, we begin to get a feel for the dynamics and start to see the formation of interesting patterns and vortical structures.

EQ_2 invariance under the symmetry group S, explained in sect. 2.4, implies the existence of 4 stagnation points SP_1-SP_4, (19). In figure 3b the view from figure 3a has been rotated in order to reveal two of these stagnation points. The visualization of the behavior of trajectories near these fixed points reveals their qualitative nature. The point at $3L_z/4$ in figure 3b appears to be an unstable spiral, whereas the point at $L_z/4$ is hyperbolic. In order to verify these hypotheses, eigenvalues and stable/unstable manifolds for these stagnation points are computed.

Linearization and Stability

For a perturbation $\delta\mathbf{x}$ away from one of the stagnation points, the change in the velocity field is given by $\delta\mathbf{u} = A\delta\mathbf{x}$ where A is the nine component velocity gradients matrix defined by $A_{ij} = \frac{\partial u_i}{\partial x_j}$. Since $\mathbf{u}$ is given by (5), it is a relatively simple extension of this formula to evaluate these partials. To find $\partial\mathbf{u}/\partial y$, one needs to use the relation $\frac{\partial}{\partial y}T_n(y) = nU_{n-1}(y)$ where T_n is the nth Chebyshev polynomial of the first kind and U_n is the nth Chebyshev polynomial of the second kind. Everything else is straightforward. The eigenvalues of A, evaluated at a stagnation point, determine local stability and reveal the qualitative nature of the motion nearby the stagnation point. For the stagnation points SP_1 - SP_4, the eigenvalues, eigenvectors, and velocity
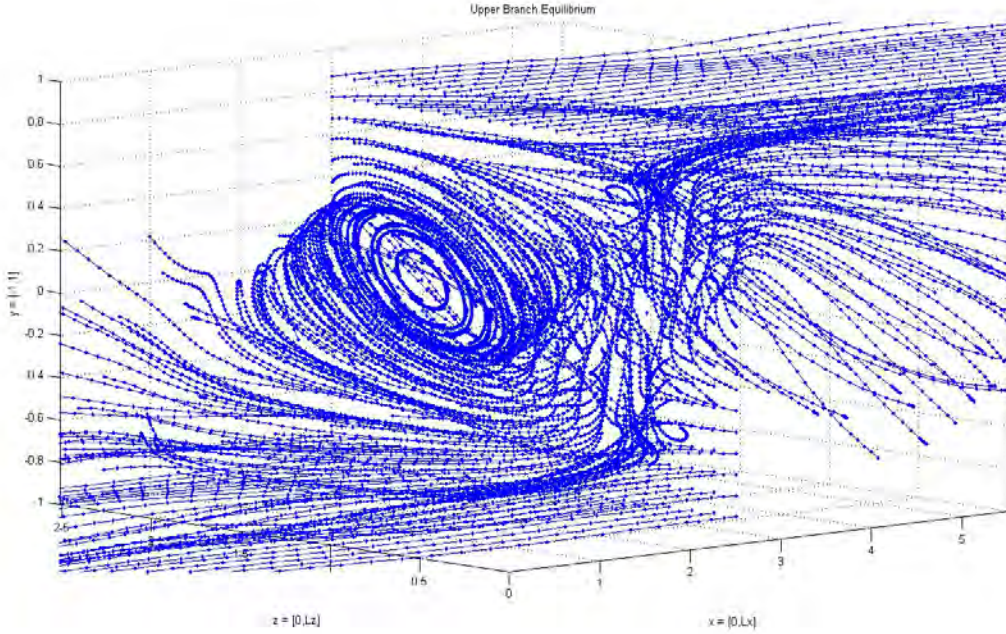
(a) $3D$ perspective view
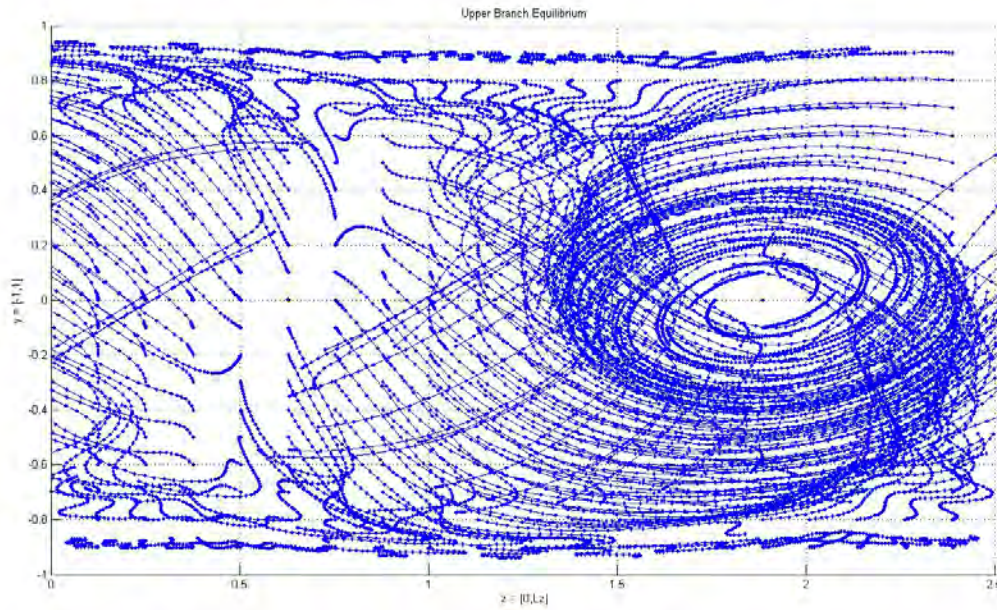
(b) Rotated to show the 2 stagnation points

Figure 3: Grid of 19×19 initial points in the $[y, z]$ plane, centered at $x = L_x/2$; integrated for 15 time units to produce tracer particle trajectories for EQ_2.

gradients matrices are as follows.

$\mathbf{x}_{SP_1} = (L_x/2, 0, L_z/4)$: There are 3 real eigenvalues, two positive and one negative.

$$\lambda^{(1)} = -0.4652099\,, \quad \mathbf{e}^{(1)} = \begin{pmatrix} 0.9844417 \\ 0.1743315 \\ 0.0219779 \end{pmatrix} \tag{36}$$

$$\lambda^{(2)} = 0.4008961\,, \quad \mathbf{e}^{(2)} = \begin{pmatrix} 0.5704000 \\ -0.7666749 \\ 0.2947091 \end{pmatrix} \tag{37}$$

$$\lambda^{(3)} = 0.0643139\,, \quad \mathbf{e}^{(3)} = \begin{pmatrix} 0.4082166 \\ 0.7525949 \\ 0.5166819 \end{pmatrix} \tag{38}$$

$$\tag{39}$$

The velocity gradients matrix is

$$A = \begin{pmatrix} -0.4305385 & -0.3002042 & 0.8282447 \\ -0.1221356 & 0.2456107 & -0.1675796 \\ 0.0001651 & -0.0828951 & 0.1849278 \end{pmatrix} \tag{40}$$

8

The point is a saddle; it has 1 stable dimension and a $2D$ plane of instability spanned by $\mathbf{e}^{(2)}$ and $\mathbf{e}^{(3)}$, with the eigenvalues summing to 0, as required by a volume-preserving flow.

The stagnation point SP_4 at $(0, 0, 3L_z/4)$ has the same eigenvalues as for SP_1. It's eigenvectors and velocity gradients matrix differ by a minus sign in the third component (except for A_{33} where the two minuses cancel).

$\mathbf{x}_{SP_2} = (L_x/2, 0, 3L_z/4)$: There is one real, negative eigenvalue and a complex pair with positive real part.

$$\lambda^{(1)} = -0.0352362, \quad \mathbf{e}^{(1)} = \begin{pmatrix} -0.9452459 \\ -0.1893368 \\ -0.2658228 \end{pmatrix} \tag{41}$$

$$\mu^{(2)} \pm i\,\omega^{(2)} = 0.0176181 \pm i\,0.0862176 \tag{42}$$

$$\mathbf{e}^{(2)} = \begin{pmatrix} 0.3737950 + 0.0544113i \\ 0.2098940 - 0.4925773i \\ 0.7554000 \end{pmatrix}, \quad \mathbf{e}^{(3)} = \begin{pmatrix} 0.3737950 - 0.0544113i \\ 0.2098940 + 0.4925773i \\ 0.7554000 \end{pmatrix}.$$

The velocity gradients matrix is

$$A = \begin{pmatrix} -0.0316935 & -0.0708737 & 0.0378835 \\ -0.0250579 & -0.0218884 & 0.0795969 \\ 0.0014742 & -0.1320575 & 0.0535818 \end{pmatrix} \tag{43}$$

Trajectories starting near this stagnation point spiral out in a plane spanned by the complex pair of eigenvectors. The stable direction is one-dimensional and points primarily along the x direction.

SP_3 at $(0, 0, L_z/4)$ has the same eigenvalues as SP_2 and again, the velocity gradients matrix is the same except for sign changes in the third component. This follows from the plane Couette symmetries.

Additional Stagnation Points

Having analyzed stagnation points SP_1-SP_4, before further investigating the dynamics, it is natural to wonder whether other such stagnation points may exist that do not necessarily follow from a symmetry argument. To answer this question, as mentioned above, we numerically compute $|\mathbf{u}|^2$ along a fine grid and look for where it's value falls below a given threshold.

We create a more refined grid of velocities which is $144 \times 105 \times 144$. This is three times the $48 \times 35 \times 48$ grid in each dimension used to show the initial tracer trajectories, and contains about 2.2 million points. At each point $|\mathbf{u}|^2$ is then calculated and at every point that satisfies $|\mathbf{u}|^2 < \epsilon$ for some arbitrarily chosen ϵ, the point is plotted.

In figure 4 we show regions in the cell where $|\mathbf{u}|^2$ is very small for $\epsilon = 10^{-4}$, notated by the globs of blue dots. The trajectories shown along with the points of small velocity in this figure, explained below, are also suggestive of the existence of a stagnation point within the spiraling region. The four previously known stagnation points are identified in the figure, but we also see a couple of additional clumps. Honing in one of the suspicious clusters, starting from the gridpoint value with smallest velocity in the suspicious region, $\mathbf{x}_0 \approx (2.33476, 0.40952, 0.64577)$, and its reflection through $\mathbf{x}_{SP_1}$, $\mathbf{x}_0' = 2\mathbf{x}_{SP_1} - \mathbf{x}_0$, the Newton iteration

$$\mathbf{x}_{k+1} = \mathbf{x}_k - A^{-1}(\mathbf{x}_k)\,\mathbf{u}(\mathbf{x}_k) \tag{44}$$

converges rapidly to verify *another* pair of stagnation points. Because we have already used notation to define points SP_1-SP_8 in sect. 2.4, we refer to these new numerically discovered stagnation points as SP_{N1} and SP_{N2}:

$$\mathbf{x}_{SP_{N1}} = (2.35105561774981, 0.42293662349708, 0.65200166068573) \tag{45}$$

$$\mathbf{x}_{SP_{N2}} = (3.16051044117966, -0.42293662349708, 0.60463540075018). \tag{46}$$

We see the symmetry in the y-component of this pair, and in fact these points are shown to be symmetric about the point SP_1, as discussed in sect. 2.4:

$$(\mathbf{x}_{SP_{N1}} + \mathbf{x}_{SP_{N2}})/2 = \mathbf{x}_{SP_1}. \tag{47}$$

Repeating the linear stability analysis for SP_{N1} and SP_{N2}: There is one real, positive eigenvalue and a complex pair with negative real part.
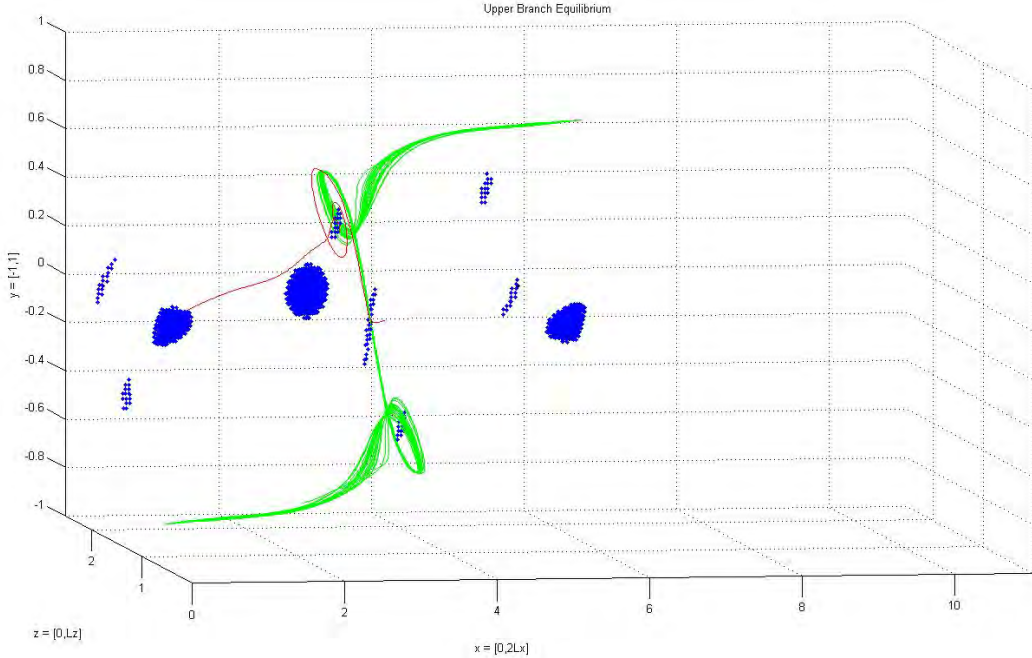
9

Figure 4: Blue clumps of points indicate where the velocity for EQ_2 is very close to zero. Shown along with the stable manifold of SP_3 and the unstable manifold of SP_1.

$$\lambda^{(1)} = 0.1453207\,, \quad \mathbf{e}^{(1)} = \begin{pmatrix} 0.9307982 \\ 0.3502306 \\ 0.1046576 \end{pmatrix} \tag{48}$$

$$\{\lambda^{(2)}, \lambda^{(3)}\} = \mu^{(2)} \pm i\,\omega^{(2)} = -0.0726603 \pm i\,0.3733478$$

$$\mathbf{e}^{(2)} = \begin{pmatrix} 0.5226203 \\ -0.6703938 \\ 0.2065610 \end{pmatrix}, \quad \mathbf{e}^{(3)} = \begin{pmatrix} 0.3779843 \\ 0 \\ -0.3031510 \end{pmatrix}. \tag{49}$$

The velocity gradients matrix is

$$A = \begin{pmatrix} 0.0225166 & 0.0985763 & 0.7623083 \\ 0.1714566 & -0.1275193 & -0.6118476 \\ -0.0615378 & 0.1755954 & 0.1050028 \end{pmatrix}. \tag{50}$$

We have this time a $1D$ unstable manifold and a $2D$ spiraling stable manifold. The trajectories shown in figure 4, which originate close to SP_1 and $SP3$, wander close to the spiraling stable manifold of the numerically discovered SP_{N1}, showing how the dynamics tends to be dominated by these stagnation points.

We have been describing all stagnation points which are inside a single periodic cell with dimensions $L_x \times 2 \times L_z$, pictured in figure 5. However even within this cell there is a redundancy in labeling all of these points as distinct. The interesting dynamics and connections between the different stagnation points occur along the x direction. To understand what is happening one needs to look only at a subset of these stagnation points that lies in the right or left half of the box, that is, in the interval $[0, L_z/2]$ or the interval $[L_z/2, L_z]$. We have chosen the interval $[0, L_z/2]$. In the x direction the most convenient interval is not actually $[0, L_x]$, rather we look at the stagnation points in the open interval $(-L_x/2, L_x)$, open so as to ignore the repeated translations on the boundary. Thus an alternate domain of investigation that will be convenient to sometimes use is

$$\Omega = (-L_x/2, L_x) \times [-1, 1] \times [0, L_z/2]. \tag{51}$$

Within this domain Ω there are then just four stagnation points. They are SP_1, SP_3, SP_{N1}, and SP_{N2}, shown in figure 6. Note that SP_{N2} is a translated version from the way it was viewed in figure 5. The phase portrait of fundamental dynamics for EQ_2 will be viewed in Ω.

Phase portrait and heteroclinic connections

With identification of all of the stagnation points within either the original periodic box or the cell Ω, as well as the corresponding linear stability analysis, we are ready to make a complete phase space portrait for the Upper Branch, EQ_2.
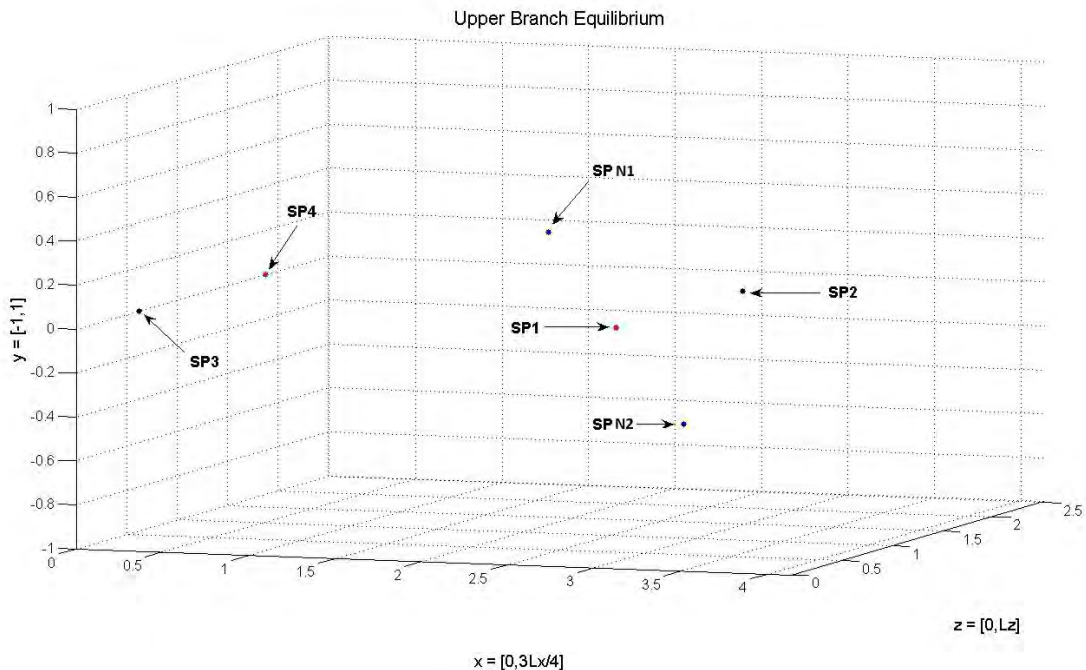
Figure 5: The 6 unique stagnation points within one periodic box for EQ_2. SP_1-SP_4 are guaranteed by EQ_2 symmetries, SP_{N1} and SP_{N2} are determined numerically.
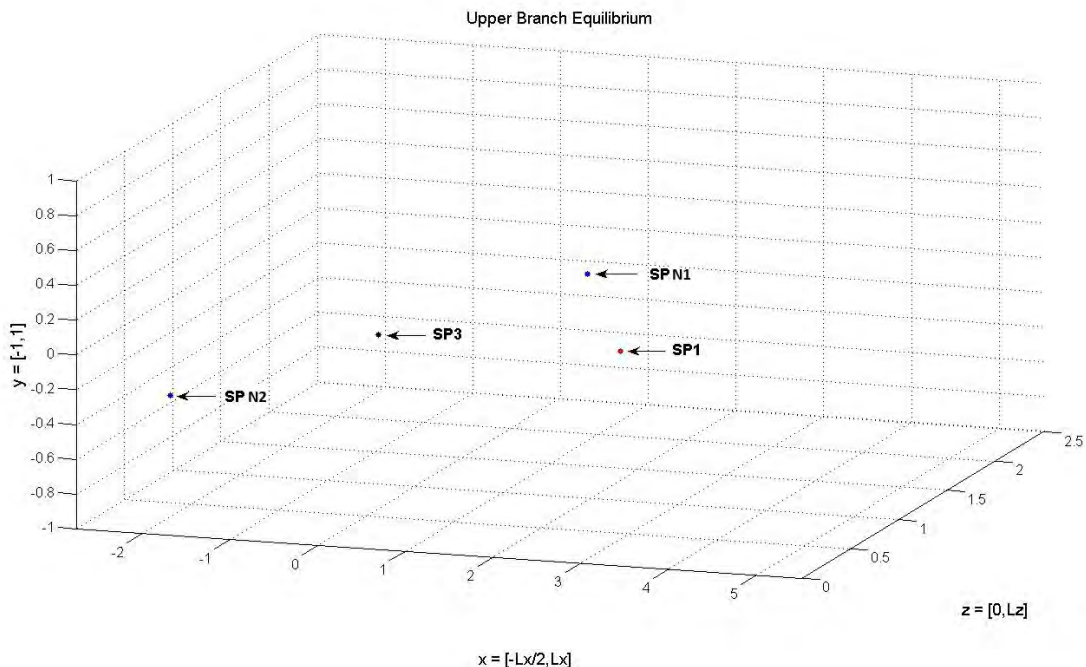

Figure 6: The 4 stagnation points that occur within the domain Ω.

The dynamics between the stagnation points and their translations is quite interesting. In figure 7 we see a partial view of the stable and unstable manifolds of two of the stagnation points, SP_1 and SP_2, in the original periodic domain, found by integrating trajectories near the fixed points forwards and backwards in time along the stable or unstable eigenvectors. Local stability analysis shows that SP_1 has all real eigenvalues with a $1D$ stable manifold, and a $2D$ unstable manifold which is locally a plane (37)-(39). The fact that one of the eigenvalues for the unstable manifold of SP_1 is much larger than the other is apparent in the figure by the fact that the trajectories in the unstable plane become quickly contracted in one of the dimensions, and the trajectories appear to leave along a nearly one-dimensional structure in the y-direction. SP_2 has a $2D$ unstable manifold with complex eigenvalues which spiral out in a plane and a $1D$ stable manifold.

As alluded to in figure 4, SP_{N1} and SP_{N2} sit near the center of the swirl of green coming from the unstable direction of SP_1. To better understand what is happening here, referring to figure 8, we compute the stable and unstable manifolds of SP_{N1} and SP_{N2}, where we use the shifted translation of SP_{N2}, along with the stable and unstable manifolds of SP_3. The blue surface is formed by the overlap of trajectories starting along the unstable manifold of SP_3 and the stable manifolds of SP_{N1} and SP_{N2}. We see that the stable manifold of SP_3 (shown by the red curves) corresponds with the unstable manifolds of SP_{N1} and SP_{N2}, thus we have *heteroclinic connections* from $SP_{N1} \to SP_3$ and $SP_{N2} \to SP_3$! The thick appearance of the red curves is simply so that they can be seen within the blue surface. They are actually just a single trajectory.

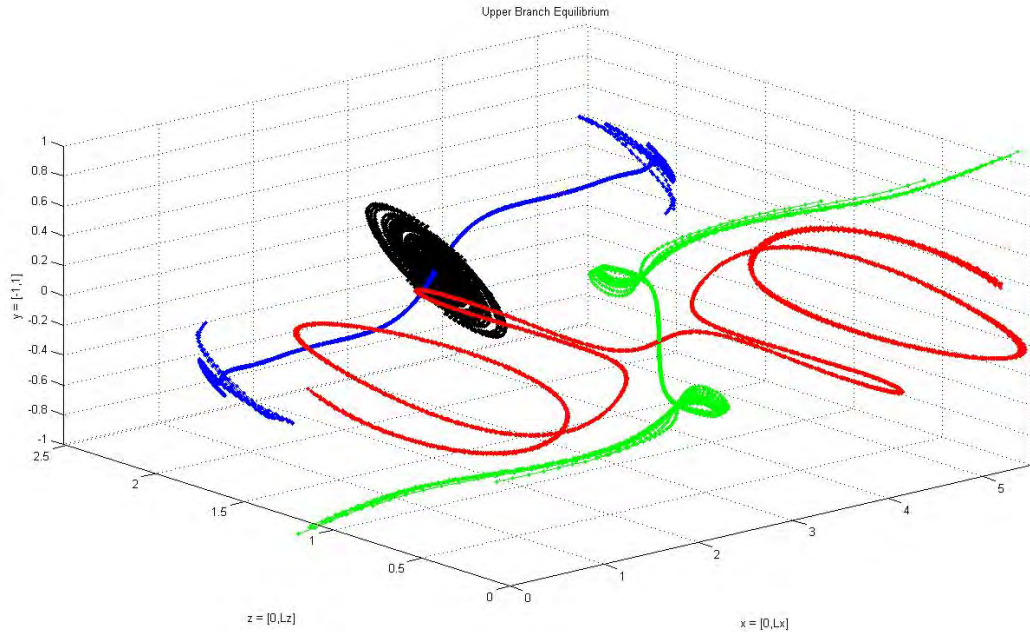Next we bring trajectories originating near SP_1 into the picture to see how the manifolds of this stagna-

Figure 7: Segments of the stable (red/blue) and unstable (green/black) manifolds of the stagnation points $\mathbf{x}_{SP_1} = (L_x/2, 0, L_z/4)$ and $\mathbf{x}_{SP_2} = (L_x/2, 0, 3L_z/4)$ for EQ_2.
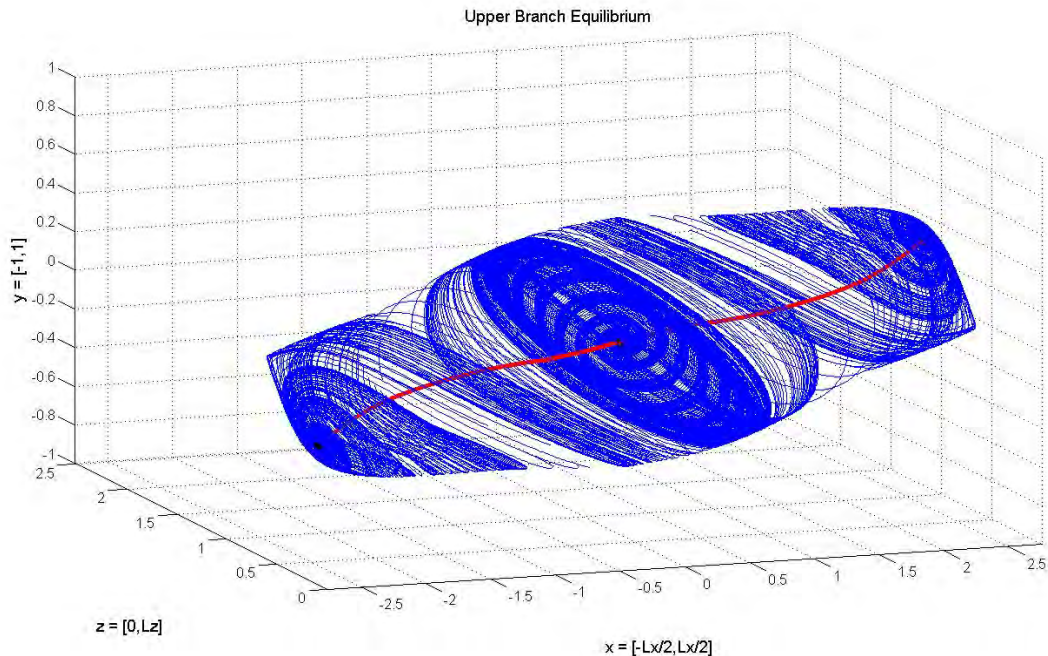

Figure 8: Heteroclinic connections of the Upper Branch (red trajectories) from SP_{N1} -> SP_3 and SP_{N2} -> SP_3, shown in a cell with $x \in$ [-$L_x/2$, $L_x/2$] along with the unstable manifold of SP_3.

tion point connect with those in figure 8, producing the full dynamical portrait within Ω. The result is shown in figure 9. Compare to figure 6 to see the locations of the stagnation points. The relation of the stable manifold of SP_1 (yellow curve) and the trajectories that are driven away from SP_1 in the unstable direction (green) to those of the blue surface is quite interesting. These trajectories tightly hug the blue surface as they spiral around it, appearing to be shielded from entering the volume it encompasses. This could have significant implications for the consideration of fluid mixing within plane Couette flow, perhaps showing that it is difficult to achieve a uniformly mixed space for this particular equilibrium; a blob of ink that starts outside of the blue surface may have a difficult time ever entering the region!

One merely translates the image in figure 9 in the x direction by an amount L_x to give a complete picture in any periodic cell. The same picture will also occur symmetrically (translated by $L_x/2$ and $L_z/2$) in the left half of the box.

3.2   Equilibrium EQ_8: Additional Symmetries

Having analyzed the Upper Branch equilibrium EQ_2, we next look at EQ_8, another equilibrium velocity field of plane Couette flow which exhibits turbulent behavior at a lower Reynolds number, 270.
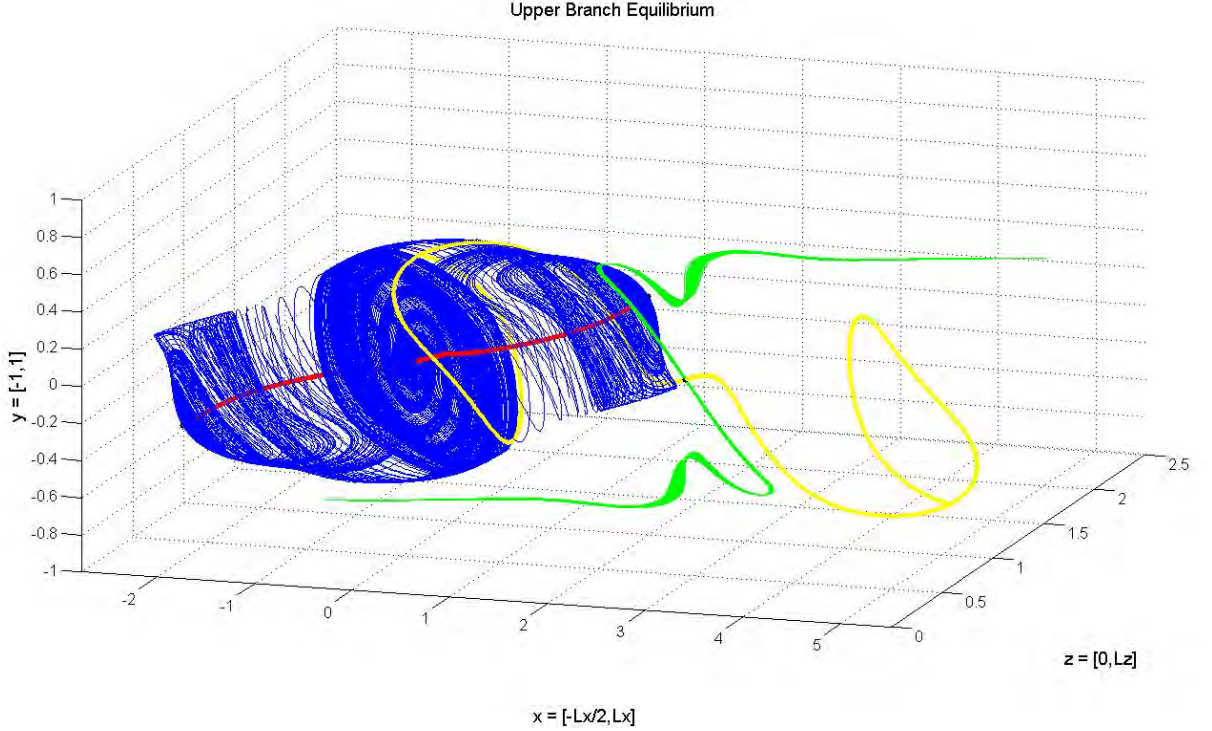
Tracer dynamics and analysis

12

Figure 9: Portrait of the fundamental dynamics along the manifolds of stagnation points SP_1, SP_3, SP_{N1}, SP_{N2} within cell Ω for the Upper Branch.

We start once again with a cleverly chosen grid of initial trajectories to get a feel for the significant structures in the flow. The grid is in a plane at $x = L_x/2$. The result, after a short integration time, is shown in figure 10. This perspective view already shows us quite a bit of information. Once again we have symmetries abound, and we know from the discussion in sect. 2.4 that there will be at least 8 stagnation points SP_1-SP_8. Another interesting feature of this plot is the four vortical structures on the left half. One final noteworthy point from the figure is the appearance of a perfect line segment connecting two of the stagnation points, which happen to be SP_1 and SP_2. This strongly suggests a heteroclinic connection between these two stagnation points. To confirm, we compute the eigenvalues and eigenvectors of the velocity gradients matrix. For SP_1, there is indeed a real, unstable eigenvector pointing along (0,0,1) and for SP_2 there is a real, stable eigenvector pointing along (0,0,1). This, together with the plot, numerically confirms the existence of the heteroclinic trajectory. The same result holds for the shifted pair at $x = 0$. The rest of the eigenvalues/eigenvectors are given below. We note that for EQ_8 there is a heteroclinic connection which is a simple horizontal line connecting the pair of trivial stagnation points in the *spanwise* direction, whereas for EQ2 the connection was some arbitrary-looking curve in the *streamwise* direction connected to a nontrivial stagnation point. Factorization of the SP_1 and SP_2 stability eigenspaces for EQ_8 occurs because the spanwise z direction is a $1D$ flow-invariant subspace at the stagnation points [20]. That ensures the simplicity of the heteroclinic connection.

EQ_8, SP_1: There are two real, positive eigenvalues and one real, negative eigenvalue.

$$\left(\lambda^{(1)}, \lambda^{(2)}, \lambda^{(3)}\right) = (0.363557, 0.227831, -0.591389) \tag{52}$$

$$\left(\mathbf{e}^{(1)}, \mathbf{e}^{(2)}, \mathbf{e}^{(3)}\right) = \left(\begin{pmatrix} 0 \\ 0 \\ 1 \end{pmatrix}, \begin{pmatrix} -0.733415 \\ -0.679780 \\ 0 \end{pmatrix}, \begin{pmatrix} 0.991005 \\ 0.133824 \\ 0 \end{pmatrix}\right).$$

EQ_8, SP_2: There are two real, positive eigenvalues and one real, negative eigenvalue.

$$\left(\lambda^{(1)}, \lambda^{(2)}, \lambda^{(3)}\right) = (0.992857, 0.255973, -1.248830) \tag{53}$$

$$\left(\mathbf{e}^{(1)}, \mathbf{e}^{(2)}, \mathbf{e}^{(3)}\right) = \left(\begin{pmatrix} 0.116961 \\ -0.993136 \\ 0 \end{pmatrix}, \begin{pmatrix} 0.957795 \\ 0.287450 \\ 0 \end{pmatrix}, \begin{pmatrix} 0 \\ 0 \\ 1 \end{pmatrix}\right). \tag{54}$$

More symmetries –> More stagnation

Equilibrium EQ_8 (as well as EQ_7, not discussed here), possesses additional symmetries compared to EQ_2. EQ_2 is in the S-invariant subspace of velocity fields and EQ_8 is in S_8 (sect. 2.3 and sect. 2.4). From (18) and (19) we know then that for EQ_8 we will have the additional stagnation points:
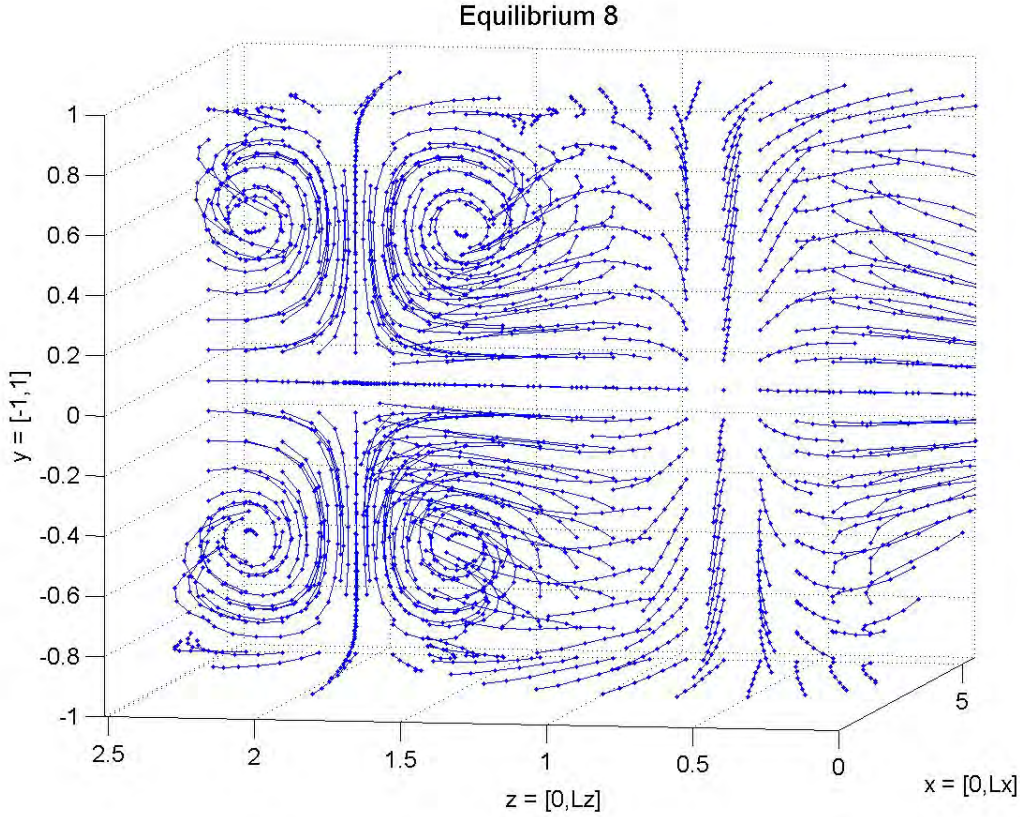
13

Figure 10: Grid of initial points in the $[y, z]$ plane, centered at $x = L_x/2$; integrated to produce tracer particle trajectories for EQ_8.

$$
\begin{aligned}
\mathbf{x}_{SP_5} &= (L_x/4, 0, 0) \\
\mathbf{x}_{SP_6} &= (3L_x/4, 0, 0) \\
\mathbf{x}_{SP_7} &= (L_x/4, 0, L_z/2) \\
\mathbf{x}_{SP_8} &= (3L_x/4, 0, L_z/2).
\end{aligned}
\tag{55}
$$

Interestingly these were actually discovered numerically *before* the symmetry arguments were understood. A Newton search on regions of very low velocity for EQ_8 revealed that $(L_x/4, 0, L_z/2)$ and $(3L_x/4, 0, L_z/2)$ are stagnation points. From this, one may deduce that symmetry s_5 must hold, and it can then be checked that at any position the velocity field is indeed invariant under s_4 and s_5.

Stability analysis of the additional set of stagnation points for EQ_8 gives the following.

SP_5: There is one real, positive eigenvalue and a complex pair with negative real part.

$$
\lambda^{(1)} = 0.03109, \quad \mathbf{e}^{(1)} = \begin{pmatrix} 0.85275 \\ 0.41774 \\ -0.31355 \end{pmatrix}
\tag{56}
$$

$$
\{\lambda^{(2)}, \lambda^{(3)}\} = \mu^{(2)} \pm i\,\omega^{(2)} = -0.01555 \pm i\,0.59385
\tag{57}
$$

$$
\mathbf{e}^{(2)} = \begin{pmatrix} 0.24762 \\ -0.31442 \\ 0.69906 \end{pmatrix}, \quad \mathbf{e}^{(3)} = \begin{pmatrix} -0.20793 \\ 0.55489 \\ 0 \end{pmatrix}.
\tag{58}
$$

We have a $1D$ unstable manifold and a $2D$ inward-spiral stable manifold. All four of the new points have the same eigenvalues. SP_5 and SP_8 have the same eigenvectors, as do SP_6 and SP_7 whose eigenvectors differ from SP_5 only by the sign of the third component for $\mathbf{e}^{(1)}$ and by the sign of the first and second components for $\mathbf{e}^{(2)}$ and $\mathbf{e}^{(3)}$.

As a final interesting side consequence of numerically searching for stagnation points for EQ_8, the figures produced by plotting gridpoints where velocity is small, using a cutoff value of $|\mathbf{u}|^2$ which is too large to actually be useful for finding stagnation points, we instead find a plot showing more intricate patterns in the flow. figure 11a shows a $3D$ perspective view of these points, and figure 11b shows the projection of figure 11a onto the xz plane. This volume-preserving flow (area preserving in Poincaré sections) may have invariant tori which, being quasiperiodic, would not be detected by the stagnation point searching routines. Though the structures in the projection plot in figure 11b are not actual tracer trajectories, they are suggestive that a search for such invariant tori in future work may be a fruitful endeavor.
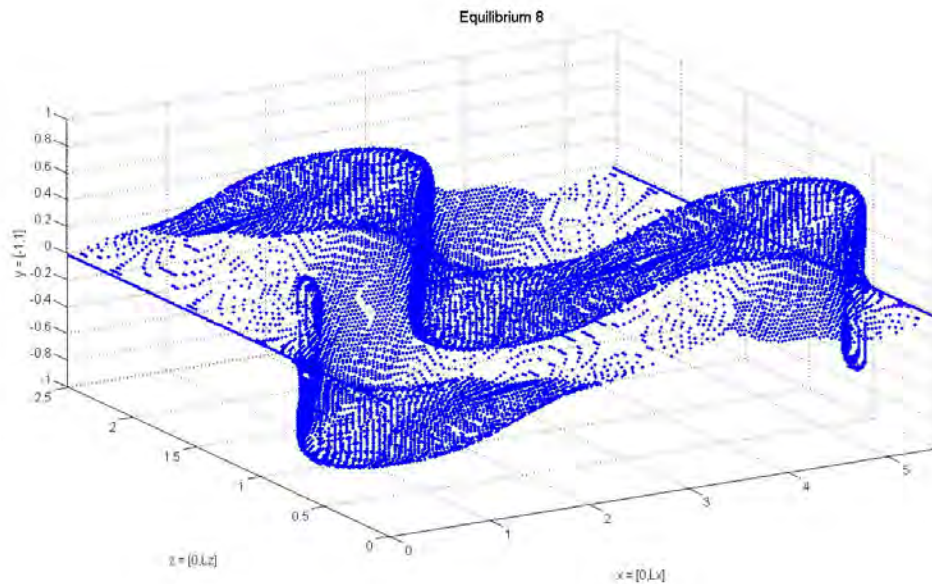
(a) Perspective view.
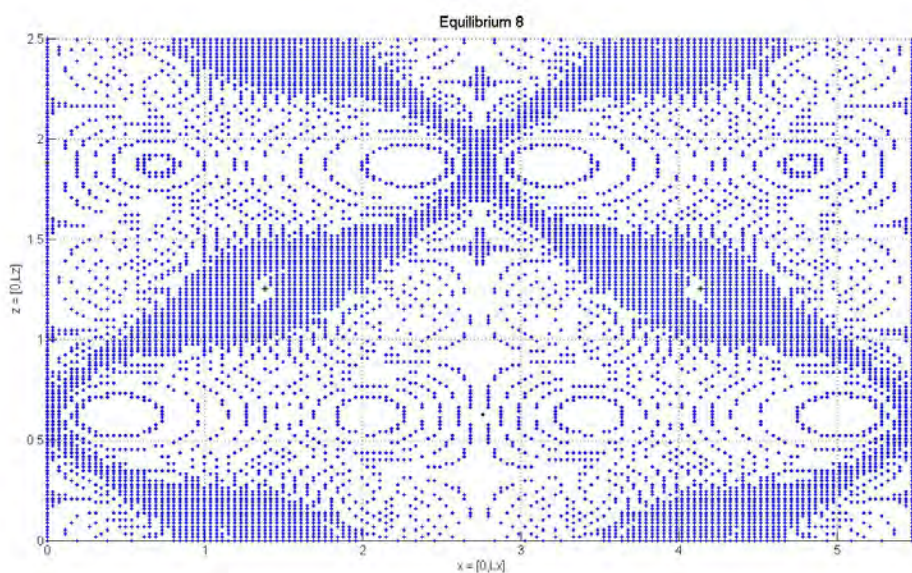
(b) Projection onto the xz plane.

Figure 11: A plot of points where the velocity field falls below a small cutoff for EQ_8, showing interesting structures in the flow.

4   Conclusion

We have taken a step towards a deeper understanding of the turbulent fluid flow in a $3D$ system from the Lagrangian perspective by studying tracer trajectory dynamics in plane Couette geometry. Potential applications that could follow from having a grasp of the Lagrangian dynamics and being able to accurately compute tracer particle trajectories are wide-ranging: velocity profile statistics or correlation functions taken over an ensemble of particle trajectories within different regions, calculations of mixing time and diffusion properties for the flow, Lyapunov exponents and material stretching, striation thickness, among others, are some of the various possible measures of chaotic advection that could be investigated. By extending the dynamical systems methods that are often confined to simpler $2D$ systems to the $3D$ world of plane Couette flow, we encounter complex coherent structures that partition the physical space of the fluid into regions which exhibit distinct types of motion and allow us to visualize the fundamental motions driven by trajectories which lie close to invariant manifolds. Relying on the symmetries of the geometry to shine light upon the situation and guide us, we are able to construct phase portraits for plane Couette equilibria starting with the identification and stability determination of stagnation or fixed points of the system. Future work could easily extend these analyses to additional invariant solutions for plane Couette flow, or apply the same methods in other fluid systems which likely posses symmetries.

5   Acknowledgments

Acknowledge group members not included as authors.

References

[1] G. Mathew, I. Mezić, and L. Petzold. A multiscale measure for mixing. *Physica D*, 211:23–46, 2005.

[2] M. Mathur, G. Haller, T. Peacock, J. E. Ruppert-Felsot, and H. L. Swinney. Uncovering the Lagrangian skeleton of turbulence. *Phys. Rev. Lett.*, 98:144–502, 2007.

[3] A. Arneodo, R. Benzi, J. Berg, L. Biferale, E. Bodenschatz, A. Busse, E. Calzavarini, B. Castaing, M. Cencini, L. Chevillard, R. Fisher, R. Grauer, H. Homann, D. Lamb, A. S. Lanotte, E. Leveque, B. Luethi, J. Mann, N. Mordant, W.-C. Mueller, S. Ott, N. T. Ouellette, J.-F. Pinton, S. B. Pope, S. G. Roux, F. Toschi, H. Xu, and P. K. Yeung. Universal intermittent properties of particle trajectories in highly turbulent flows. *Phys. Rev. Lett.*, 100:254504, 2008.

[4] W. Braun, F. De Lillo, and B. Eckhardt. Geometry of particle paths in turbulent flows. *J. Turbul.*, 7:N62, 2006.

[5] N. Mordant, E. Lévêque, and J. Pinton. Experimental and numerical study of the Lagrangian dynamics of high Reynolds turbulence. *New J. Phys.*, 6:116–116, 2004.

[6] J. M. Ottino. *The Kinematics of Mixing: Stretching, Chaos and Transport*. Cambridge Univ. Press, Cambridge UK, 1989.

[7] S. Wiggins. *Chaotic Transport in Dynamical Systems*. Springer, N.Y., 1992.

[8] G. Haller. Lagrangian coherent structures from approximate velocity data. *Phys. Fluids*, 14:1851–1861, 2002.

[9] N. F.s Egenti and U. H. Chimezie. The turbulent Lagrangian dissipative particle velocity statistics. *Mediterranean J. Basic. Appl. Sci.*, 6:84–92, 2022.

[10] G. Falkovich, K. Gawedzki, and M. Vergassola. Particles and Fields in Fluid Turbulence. *Rev. Mod. Phys.*, 73:913–975, 2001.

[11] J. Halcrow, J. F. Gibson, P. Cvitanović, and D. Viswanath. Heteroclinic connections in plane Couette flow. *J. Fluid Mech.*, 621:365–376, 2009.

[12] D. Viswanath. The fractal property of the Lorenz attractor. *Physica D*, 190:115–128, 2004.

[13] M. Nagata. Three-dimensional finite-amplitude solutions in plane Couette flow: Bifurcation from infinity. *J. Fluid Mech.*, 217:519–527, 1990.

[14] F. Waleffe. Homotopy of exact coherent structures in plane shear flows. *Phys. Fluids*, 15:1517–1543, 2003.

[15] J. F. Gibson, J. Halcrow, and P. Cvitanović. Visualizing the geometry of state space in plane Couette flow. *J. Fluid Mech.*, 611:107–130, 2008.

[16] J. F. Gibson. Channelflow: A spectral Navier-Stokes simulator in C++. Technical report, U. New Hampshire, 2017. `Channelflow.org`.

[17] J. F. Gibson. Database of invariant solutions of plane Couette flow, 2013. `Channelflow.org/database`.

[18] J. Halcrow. *Geometry of turbulence: An exploration of the state-space of plane Couette flow*. PhD thesis, School of Physics, Georgia Inst. of Technology, Atlanta, 2008. `ChaosBook.org/projects/theses.html`.

[19] T. Sahai and A. Vladimirsky. Numerical methods for approximating invariant manifolds of delayed systems. *SIAM J. Appl. Dyn. Syst.*, 8:1116–1135, 2009.

[20] E. Siminos and P. Cvitanović. Continuous symmetry reduction and return maps for high-dimensional flows. *Physica D*, 240:187–198, 2011.